A galvanic cell oxygen analyzer

K. Mancy

Journal of Electroanalytical Chemistry (1959)

Related papers

Download a PDF Pack of the best related papers ⧉

A UNIFIED THEORY OF STREAMING MAXIMA OF FIRST AND THIRD KIND, AS WJ3LL AS OF THEI…
Rolando Guidelli

Problems in the polarography of chromate
Israel Miller

MECHANISM OF ELECl-'ROHYDRODIMERlZATlQN OF FUMARODiNlTRILE ON MERCURY FROM AQUEOUS …
Rolando Guidelli

A GALVANIC CELL OXYGEN ANALYZER

K. H. MANCY, D. A. OKUN and C. N. REILLEY

Department of Sanitary Engineering, School of Public Health, and Department of Chemistry, University of North Carolina, Chapel Hill, N.C. (U.S.A.)

INTRODUCTION

In natural waters and wastes, electrode systems such as the dropping mercury electrode[1-3] and the rotating platinum electrode[4] have been employed. Other investigators[5,6] used materials of a high hydrogen overvoltage (alloys of Fe, Cr, Ni, Sn, Sb and Pb) as cathodes to give improved sensitivity and/or accuracy in the continuous voltammetric determination of dissolved oxygen.

Oxygen determinations using galvanic systems have been successfully used in gas streams. HERSCH[7] and BAKER *et al.*[8] reported systems composed of a silver cathode and a lead anode immersed in 24 wt.% potassium hydroxide, while KEIDEL[9] also developed a sensitive instrument for trace quantities of oxygen, but based upon a silver–cadmium galvanic couple. TÖDT[10] devised a corrosion indicator which was basically a galvanic cell for oxygen measurement. In all cases, one of the principle problems has been the effect of electroactive or surface active impurities which either react with or poison the sensing device. One way to avoid the effect of such impurities is to scrub the oxygen out of the sample by a carrier gas and to measure the oxygen content in the gas phase[7].

An alternate but simple approach is accomplished by covering the sensing electrode with a membrane permeable to oxygen but non-permeable to other substances in the test solution. An early attempt in this direction was reported by KAMIENSKI[11] who employed a protective adsorption film of hydrophilic colloid (silica gel) to cover a microplatinum electrode. More recently, CLARK *et al.*[12] described a procedure for recording dissolved oxygen in blood by the use of a micro-platinum electrode covered with a polyethylene membrane. This membrane is permeable to oxygen (and other gases), but practically non-permeable to ionic species of the solution. On this basis, REEVES, RENNIE AND PAPPENHEIMER[13] tested for oxygen in urine and SUGIOKA AND DAVIES[14] monitored oxygen tension in interstitial brain fluids in dogs. The use of a plastic membrane as a selective diffusion layer also suggested the possibility of voltammetric analysis in gases. SAWYER *et al.*[15] studied different kinds of Teflon and polyethylene membranes for the quantitative measurement of oxygen and sulfur dioxide in gas mixtures. Because of the temperature dependence of oxygen diffusion in the membrane, CARRITT AND KANWISHER[16] have incorporated a thermistor in their electrode system.

Because attempts to utilize these electrode systems for oxygen determination in natural waters and wastes were unsatisfactory, a study was made to develop a more

suitable electrode system. The desired characteristics of an ideal electrode system include the ability for continuous monitoring for oxygen, long term stability, ruggedness and suitability for field use as well as unit plant processes, simplicity, ease of operation and maintenance. The resulting electrode system which has been used to advantage in several recent studies, appears to approach the desired characteristics more closely than those previously reported and its design constitutes the purpose of this report.

ELECTRODE MATERIAL

Previous studies in this laboratory on the electrolytic oxygen reduction on platinum electrodes, such as encountered in cell designs similar to that reported by CARRITT AND KANWISHER[16], showed evidence that the reaction was highly dependent on the previous history of the platinum surface. Recently LINGANE[17] showed that the reduction of oxygen on a platinum wire cathode is complex and involves the platinum–platinum oxide couple. In acid solutions the presence of platinum oxide film on the electrode surface is essential for the reduction of oxygen; in its absence the electrode reaction does not occur. Similar conclusions were substantiated by the recent studies of SAWYER AND INTERRANTE[18] on electrolytic oxygen reduction at the platinum and other electrodes. The latter authors postulated that the mechanism of the reaction proceeds through the reduction of the metal oxide which is in turn reformed by the reaction of the oxygen on the metal. If this latter reaction is slow, smaller kinetic-limited currents will be obtained. Significantly, SAWYER AND INTERRANTE reported that this phenomenon did not occur at the silver and gold electrodes. For this reason, silver was selected as the cathode material and performance characteristics more stable than with platinum were achieved.

Lead was selected as the anode material since its electrode potential is sufficiently negative to cause spontaneous reduction of oxygen but not so negative as to cause reduction of the supporting electrolyte. Also, its electrode reactions are quite reversible. With this design an external source of applied voltage is not needed and the instrument is therefore somewhat more suitable for field use. A $1 M$ potassium hydroxide solution was chosen as the supporting electrolyte because its conductivity is high, the residual current in the absence of oxygen is small and lead ions are soluble in it, thus maintaining a clean anode.

GALVANIC CELL OXYGEN ANALYZER

The cell design is shown in Fig. 1. A thin polyethylene membrane fixed in near contact with the electrode surface permits rapid diffusion of oxygen to the electrode's surface. The membrane and the thin layer of potassium hydroxide electrolyte solution constitute rigorously defined diffusion layers of constant thickness and exhibit a minimum "edge" effect. Because of the mechanical stability of this design and because of the smaller permeability of oxygen in the membrane as compared with the sample medium, the flux of oxygen and hence the current become independent of the degree of stirring in the test solution above a certain small threshold value. Two other advantages accrue from applying a polyethylene membrane over the sensing electrode. First, oxygen levels in non-conducting liquids and in gaseous streams may be measured. Second, the membrane forms a protective diffusion barrier separating the electrode system from the test sample, which, because of its high selective per-

meability towards oxygen, permits measurements for oxygen in the presence of electroactive and surface active impurities that interfere in conventional voltammetry.

The current generated in this electrode system will depend at steady state on the rate of mass transfer of the electroactive species across the membrane and on the
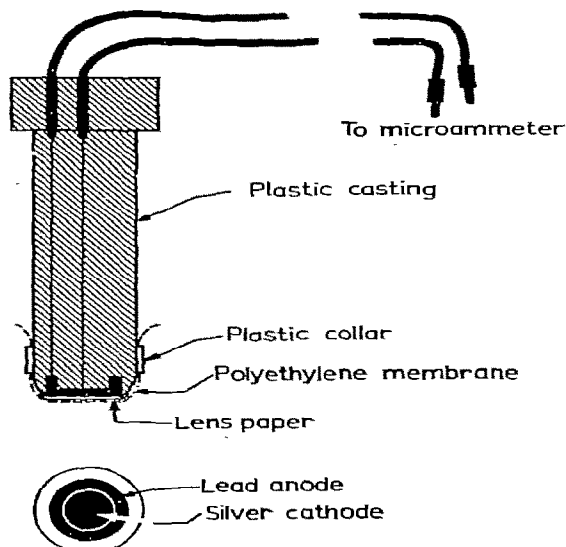

Fig. 1. The galvanic cell oxygen analyzer.

kinetics of the overall electrochemical process within the galvanic cell. When the silver cathode is used, the concentration of oxygen at the cathode surface is reduced to zero when the cell is placed in operation. Because the potassium hydroxide liquid layer is quite thin and because the permeability of oxygen in this layer is great, the rate of mass transfer across the membrane under total concentration polarization becomes the rate determining step at steady state.

STEADY STATE MASS TRANSFER THROUGH MEMBRANES

The permeability (steady state) of homogeneous polymeric, non-rigid membranes to gases and vapors is usually described[19-21] by:

$$q = P_m \frac{C_1 - C_2}{b} \tag{1}$$

where C_1 and C_2 are the surface concentrations, moles cm^{-3}, in the phases on opposite sides of the membrane, q the flux, moles cm^{-2}sec^{-1}, P_m permeability coefficient of the membrane, cm^{2}sec^{-1}, and b the membrane thickness, cm.

The permeation process through plastic membranes involves first the solution of the permeating gas in the membrane material[19,20]. Customary equilibrium conditions are assumed to prevail at the membrane–phase boundary. Thus at low concentrations

a linear relationship exists between the external gas concentration, C, and the corresponding equilibrium concentration, C_m, within the membrane surface.

$$C_m = kC \tag{2}$$

where k is the distribution coefficient.

Diffusion of the gas molecules within the membrane at steady state conditions may then be expressed as:

$$q = -D_m \frac{C_{m_1} - C_{m_2}}{b} \tag{3}$$

where D_m is the gas diffusion coefficient ($cm^2 sec^{-1}$) in the membrane, at whose surfaces are maintained constant concentrations C_{m_1} and C_{m_2} moles cm^{-3}, respectively.

From eqns. 1–3 the relationship between the permeability coefficient, P_m, and the diffusion coefficient, D_m, is:

$$P_m = kD_m \tag{4}$$

THEORY OF DIFFUSION CURRENT FOR TWO-LAYER ELECTRODE SYSTEMS

Fig. 2 illustrates schematically the arrangement of the electrode and the pertinent concentration profiles. Separating the membrane from the silver cathode is a thin film of electrolyte solution. It is assumed initially that, with the analyzer immersed in a test solution of oxygen concentration C_s, equilibrium concentrations $C_{m,0}$, $C_{f,0}$
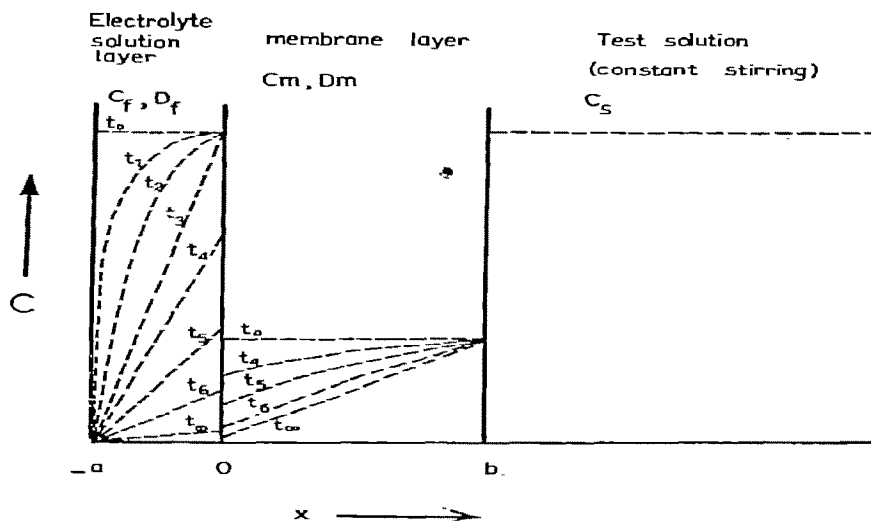

Fig. 2. Schematic diagram of theoretical steady state attainment. Concentration–distance profiles.

exist throughout the membrane and the electrolyte solution film respectively. The test solution is maintained homogeneous at all times by adequate stirring. On closing the cell circuit, the potential imposed on the cathode is sufficient to cause immediate and complete reduction of oxygen. As the time of electrolysis increases, the concen-

tration profile is continually modified until steady state, with a concentration profile corresponding to t_∞, is attained. The current is governed by the rate of diffusion of the electroactive species to the electrode surface[22] and is given by:

$$i_t = nFAD \left(\frac{\partial C}{\partial x}\right)_{x=-a}$$

(5)

where n is the number of electrons transfered in the electrode process, F the Faraday and A is the electrode surface area (silver).

In order to develop an expression for the diffusion current as a function of time, it is necessary to solve FICK's second law for linear diffusion

$$\frac{\partial C}{\partial t} = D \frac{\partial^2 C}{\partial x^2}$$

(6)

under the appropriate initial and boundary conditions and substitute the flux value obtained into eqn. 5.

Eqns. 5 and 6 have been written in terms of concentrations of the electroactive species instead of the chemical potentials in order to simplify the discussion. The effect of this will be discussed later.

In the mathematical treatment of the diffusion problem, the following assumptions are considered:

(1) The diffusing substance enters through the membrane plane face and a negligible amount through the edges.

(2) The diffusion coefficient in the electrolyte solution film, D_f, and in the membrane layer, D_m, are constant parameters independent of concentration, time, and location within the appropriate phase.

(3) Initial conditions: $t = 0$

The equivalent equilibrium concentrations are given in terms of the following partition coefficients:

(a) $k_0 = \dfrac{C_{m,0}}{C_{f,0}}$ at $x = 0$

(b) $k_b = \dfrac{C_{m,0}}{C_s}$ at $x = b$

(4) Boundary conditions:

(a) $C_f = 0$ at $x = -a$

(b) $C_f = \dfrac{C_m}{k_0}$ at $x = 0$

(c) $D_f \dfrac{dC_f}{dx} = D_m \dfrac{dC_m}{dx}$ at $x = 0$

(d) $\dfrac{\partial C_f}{\partial t} = D_f \dfrac{\partial^2 C_f}{\partial x^2}$ $-a < x < 0$

(e) $\dfrac{\partial C_m}{\partial t} = D_m \dfrac{\partial^2 C_m}{\partial x^2}$ $0 < x < b$

(f) $C_m = k_b C_s$ at $x = b$

The subscripts f, m, and s signify the electrolyte solution film, the membrane layer, and the test solution respectively. The Laplace transform is used to solve eqn. 6 under the prescribed initial and boundary conditions. The transformation gives

$$\mathscr{L}C_f = \frac{C_{f,0}}{p}\left[1 - \frac{m \sinh z\sqrt{p} + l \sinh(-\delta)\sqrt{p}}{l \sinh w\sqrt{p} + m \sinh S\sqrt{p}}\right] \tag{7}$$

$$\mathscr{L}C_m = \frac{C_{f,0}}{p}\left[k_0 + \frac{2 \sinh \dfrac{x-b}{\sqrt{D_m}}\sqrt{p}}{l \sinh w\sqrt{p} + m \sinh S\sqrt{p}}\right] \tag{8}$$

where $\mathscr{L}C_f$ = the Laplace transform for C_f;

$\quad\mathscr{L}C_m$ = the Laplace transform for C_m;

$\quad p$ = the Laplace transform constant;

$$m = \left(\frac{1}{k_0} - \sqrt{\frac{D_m}{D_f}}\right); \qquad\qquad S = \left(\frac{a}{\sqrt{D_f}} - \frac{b}{\sqrt{D_m}}\right);$$

$$l = \left(\frac{1}{k_0} + \sqrt{\frac{D_m}{D_f}}\right); \qquad\qquad -\delta = \left(\frac{b}{\sqrt{D_m}} - \frac{x}{\sqrt{D_f}}\right);$$

$$w = \left(\frac{a}{\sqrt{D_f}} + \frac{b}{\sqrt{D_m}}\right); \qquad\qquad z = \left(\frac{x}{\sqrt{D_f}} + \frac{b}{\sqrt{D_m}}\right).$$

The inverse Laplace transformations of eqns. 7 and 8 yield the concentration of the diffusing substance at a distance x from the electrode surface at time t in the electrolyte solution film and in the membrane layer respectively:

$$C_f(x,t) = C_{f,0}[1 - (\gamma_1 + \gamma_2)] \tag{9}$$

where

$$\gamma_1 = \left(\frac{-\delta}{w}\right) + \frac{2}{\pi}\sum_{j=0}^{\infty}(-1)^j \frac{\sin j\pi\left(\dfrac{-\delta}{w}\right)}{j} e^{-\frac{j^2\pi^2 t}{w^2}}$$

$$+ \frac{m}{l}\frac{2\pi}{w^2}\int_0^t\left[\left\{\frac{S}{w} + \frac{2}{\pi}\sum_{n=0}^{\infty}\frac{(-1)^n}{n}\sin\left(\frac{n\pi S}{w}\right)e^{-\frac{n^2\pi^2(t-z)}{w^2}}\right\}\right.$$

$$\left.\left\{\sum_{i=0}^{\infty}(-1)^{i+1}i\, e^{-\frac{\pi^2 i^2 z}{w^2}}\sin\left(\frac{i\pi(-\delta)}{w}\right)\right\}\right]dZ$$

$$\gamma_2 = \frac{m}{l}\int_0^t\frac{2\pi}{w}\sum_{j=0}^{\infty}(-1)^j\, je^{-\frac{\pi^2 j^2(t-\varepsilon)}{w^2}}\sin\left(\frac{j\pi z}{w}\right)d\varepsilon$$

$$+ \left(\frac{m}{l}\right)^2\frac{2\pi}{w^2}\int_0^t\left[\left\{\frac{S}{w} + \frac{2}{\pi}\sum_{n=0}^{\infty}\frac{(-1)^n}{n}\sin\left(\frac{\pi n S}{w}\right)e^{-\frac{n^2\pi^2(t-\varepsilon)}{w^2}}\right\}\right.$$

$$\left.\left\{\sum_{i=0}^{\infty}(-1)^{i+1}i\sin\left(\frac{i\pi z}{w}\right)e^{-\frac{i^2\pi^2\varepsilon}{w^2}}\right\}\right]d\varepsilon$$

$$C_m(x,t) = C_{f,0}[k_0 - 2\gamma_3] \tag{10}$$

where

$$\gamma_3 = \frac{1}{l}\left[\frac{\frac{b-x}{\sqrt{D_m}}}{w} + \frac{2}{\pi}\sum_{n-0}^{\infty}(-1)^n\sin\left(n\pi\frac{\frac{b-x}{\sqrt{D_m}}}{w}\right)e^{-\frac{n^2\pi^2 t}{w^2}}\right.$$

$$+\frac{m}{l}\left\{\frac{2\pi}{w^2}\int_0^t\left(\frac{S}{w} + \frac{2}{\pi}\sum_{j-0}^{\infty}\frac{(-1)^j}{j}\sin\left(\frac{j\pi S}{w}\right)e^{-\frac{j^2\pi(t-Z)}{w^2}}\right)\right.$$

$$\left.\left.\left(\sum_{i-0}^{\infty}(1-)^{l+1}ie^{-\frac{i^2\pi^2 z}{w^2}}\sin\left(i\pi\frac{\frac{b-x}{\sqrt{D_m}}}{w}\right)\right)\,dZ\right\}\right]$$

Since the diffusion current is governed by the flux at the electrode surface, the problem at hand is to obtain an expression for the concentration gradient at any instant and at $x = -a$, from which, by means of eqn. 5, the current can be computed. Because of the complex nature of the general solution (eqns. 9 and 10), the following special conditions are considered.

(1) $\dfrac{a}{\sqrt{D_f}} = \dfrac{b}{\sqrt{D_m}}$

$$\left(\frac{\partial C_f}{\partial x}\right)_{x--a} = \frac{C_{f,0}}{a}\left[\sum_{n-0}^{\infty}\left((-1)^n\frac{\left(\frac{1}{k_0} - \sqrt{\frac{D_m}{D_f}}\right)}{\left(\frac{1}{k_0} + \sqrt{\frac{D_m}{D_f}}\right)} + 1\right)e^{-\frac{n^2\pi^2 D_f t}{4a^2}} + \frac{\sqrt{\frac{D_m}{D_f}}}{1 + \sqrt{\frac{D_m}{D_f}}}\right] \tag{11}$$

(2) $\dfrac{a}{\sqrt{D_f}} \gg \dfrac{b}{\sqrt{D_m}}$

$$\left(\frac{\partial C_f}{\partial x}\right)_{x--a} = \frac{C_{f,0}}{a}\left\{1 + 2\sum_{n-0}^{\infty}e^{-\frac{n^2\pi^2 D_f t}{a^2}}\right\} \tag{12}$$

(3) $\dfrac{a}{\sqrt{D_f}} \ll \dfrac{b}{\sqrt{D_m}}$

$$\left(\frac{\partial C_f}{\partial x}\right)_{x--a} = \frac{C_{f,0}}{b}\left(\frac{D_m}{D_f}\right)k_0\left\{1 + 2\sum_{n-0}^{\infty}e^{-\frac{n^2\pi^2 D_m t}{b^2}}\right\} \tag{13}$$

The series terms in eqns. 11–13 converge rapidly except at short time intervals. Thus these equations are most convenient at longer times of electrolysis. On the other hand by using the error function in solving for the equations for the specified conditions, an expression for the concentration gradient at the electrode surface is obtained which is valid for small values of t:

(1) $\dfrac{a}{\sqrt{D_f}} = \dfrac{b}{\sqrt{D_m}}$

$$\left(\frac{\partial C_f}{\partial x}\right)_{x=-a} = \frac{C_{f,0}}{\sqrt{\pi t D_f}}\left[1 + 2\sum_{n=0}^{\infty} e^{-\frac{4n^2a^2}{D_f t}}\right] \tag{14}$$

(2)　$\dfrac{a}{\sqrt{D_f}} \gg \dfrac{b}{\sqrt{D_m}}$

$$\left(\frac{\partial C_f}{\partial x}\right)_{x=-a} = \frac{C_{f,0}}{\sqrt{\pi t D_f}}\left[1 + 2\sum_{n=0}^{\infty} e^{-\frac{n^2a^2}{D_f t}}\right] \tag{15}$$

(3)　$\dfrac{a}{\sqrt{D_f}} \ll \dfrac{b}{\sqrt{D_m}}$

$$\left(\frac{\partial C_f}{\partial x}\right)_{x=-a} = \frac{C_{f,0}}{\sqrt{\pi t D_f}}k_0\left(\frac{D_m}{D_f}\right)^{\frac{1}{2}}\left(1 + 2\sum_{n=0}^{\infty} e^{-\frac{n^2b^2}{D_m t}}\right) \tag{16}$$

The electrode system discussed in this paper falls under the condition $b/\sqrt{D_m} \gg a/\sqrt{D_f}$. Hence the transient current for *longer* time intervals of electrolysis can be calculated from:

$$i_t = nFA\frac{D_m k_0}{b}C_{f,0}\left\{1 + 2\sum_{n=0}^{\infty} e^{-\frac{n^2\pi^2 D_m t}{b^2}}\right\}$$

Alternatively, since

$$C_{f,0} = \frac{k_b}{k_0}C_s$$

and

$$P_m = k_b D_m$$

the equation may be written in terms of the permeability coefficient:

$$i_t = nFA\frac{P_m}{b}C_s\left\{1 + 2\sum_{n=0}^{\infty} e^{-\frac{n^2\pi^2 D_m t}{b^2}}\right\} \tag{17}$$

at *steady state*, the current is:

$$i_\infty = nFA\frac{P_m}{b}C_s \tag{18}$$

From eqns. 5 and 16 the transient current at *short* time intervals is:

$$i_t = nFA\left(\frac{P_m}{\pi t}\right)^{\frac{1}{2}}C_s\left\{1 + 2\sum_{n=0}^{\infty} e^{-\frac{n^2b^2}{D_m t}}\right\} \tag{19}$$

Eqn. 19 indicates that the current varies directly with the $\sqrt{P_m}$. At *very* small values of t, however, the electrolyte film will be of primary importance and the flux, and hence the current, will vary according to eqn. 15. Because of the nature of the assumption $(b/\sqrt{D_m} \gg a/\sqrt{D_f})$, eqn. 19 does not hold at extremely short times but only after times when diffusion in the membrane is governing.

EXPERIMENTAL

The cathode of the cell is a silver disc 0.6 cm in diameter surrounded by a ring-shaped lead anode (Fig. 1). The galvanic couple is imbedded in a solid polystyrene plastic in the shape of a probe, the tip of which is smoothed with a fine sand paper; the plastic membrane is fitted firmly against it by means of a plastic collar. Between the membrane and the surface of the galvanic couple, a thin disc of lens paper impregnated with 1.0 M solution of potassium hydroxide is placed covering both the cathode and the anode. A piece of insulating tape is then used to cover the edge of the membrane below the collar to prevent any possible contamination of the supporting electrolyte. The quantity of the electrolyte solution is estimated to be about 0.1 ml.

A 0–15 microammeter is satisfactory and, where desired, a recorder may be used. Current–time curves were obtained by the use of a Dumont Cathode Ray Oscilloscope, Type 350. Photographs of the oscillograms were made with a Polaroid Land Camera using a Polaroid film No. 42.

The polyethylene membrane used in this study was provided by Engineering Plastic, Inc., Gibsonville, N.C. It is postulated to have the following characteristics*:

density,	0.92 g/cm³;
oxygen permeability,	0.15 g/24 h/100 sq. in./atm.;
carbon dioxide permeability,	0.70 g/24 h/100 sq. in./atm.;
water vapor permeability,	0.93 g/24 h/100 sq. in./atm.;
thickness,	1.0 mil.

The thickness of the polyethylene membrane was checked by measuring ten or fifteen layers with a micrometer graduated in thousandths of an in. The average deviation in a series of such measurements was less than 1%.

RESULTS AND DISCUSSION

The main design factors that influence the performance characteristics of the membrane-analyzer are as follows:
  (1) the thickness and permeability of the plastic membrane;
  (2) the geometry and the arrangement of the galvanic couple;
  (3) the quantity of the electrolyte solution.

Membrane characteristics

A large number of membranes were tested. Some were found to be too impermeable for use. Others, such as polyethylene, polypropylene, teflon and natural rubber showed sufficient permeability towards oxygen and at the same time proved to be sufficiently impermeable to interfering ionic species in the test solution. Although these materials are actually made under widely variable manufacturing conditions, it was found that most of the commercially available polyethylene membranes are suitable.

During the mounting of the membrane it usually undergoes a certain amount of stretching which will change its thickness unevenly around the edges. However, if

* *Alanthon-Polyethylene Resin*, a booklet published by E. I. DuPont De Nemour and Co., Inc., Wilmington, Delaware.

the surface of the galvanic couple and the embedding plastic are carefully smoothed, particularly around the edges, this effect can be greatly minimized. Reproducible stretching of the mounted membrane is easily acquired after few trials.

Cell geometry

The arrangement of the galvanic couple was found to have a significant effect on the sensitivity as well as on the analyzer response time. Previous studies in this laboratory using different electrode designs showed that the arrangement of the cathode and anode and the distance separating them are important design factors. In the design shown in Fig. 1, the exposed area of the analyzer facing the test sample is equal to that of the galvanic couple. This arrangement minimized any possible lateral diffusion of the electroactive species from the sides and around the edges of the analyzer, since the lead ring removes oxygen from this source and "guards" in this way the silver disc and yet does not contribute to the measured current.

Supporting electrolyte

The silver–lead galvanic cell analyzer showed suitable sensitivity with the different supporting electrolytes as illustrated in Table I. If the test sample contains a considerable amount of carbon dioxide, it may be advantageous to use 10% sulfuric acid as supporting electrolyte in the cell although this was not checked.

TABLE I

SENSITIVITY AND RESIDUAL CURRENT AT VARYING SUPPORTING ELECTROLYTES AT 25°

Supporting electrolyte	Sensitivity $(\mu A/mg/l)$	Residual current μA
1 M KOH	1.05	0.2
10% by vol. H_2SO_4	1.12	1.2
Sat. soln. KCl	0.64	1.0
Sat. soln. $KHCO_3$	0.95	0.3

By the use of potassium hydroxide electrolyte, the silver–lead electrode system showed maximum stability, low residual current, and no apparent change in sensitivity over a wide range of the hydroxide concentration. However, at potassium hydroxide concentrations below 0.05 M the analyzer showed lower response.

The quantity and the concentration of the electrolyte are important, however. As the cell discharges, the over-all concentration of the potassium hydroxide in solution falls. Also, the carbon dioxide present in test samples is capable of penetrating through the membrane and reacting with the hydroxides forming carbonates. This leads eventually to a marked lowering of the analyzer sensitivity. Previous studies in this laboratory showed that the larger quantities of the electrolyte solution are undesirable as the residual current is higher and the electrode response to changes in the oxygen concentration in the test sample is much slower. On using a total amount of electrolyte solution estimated to be 0.1 ml, the lead–silver electrode system showed minimum residual current, a very fast response, and a reasonable life time before need for cleansing and replenishing of electrolyte.

Sensitivity and linearity of response

At 25° the sensitivity, ϕ, was 1.05 μA/mg/l dissolved oxygen. Using a 1-mil thick polyethylene membrane and 1.0 M potassium hydroxide, this sensitivity remained unchanged throughout a period of 3 weeks of continuous monitoring of oxygen in tap water. Care should be taken to prevent damage and drying of the membrane. It is advisable to store the analyzer by submerging it in a saturated solution of sodium sulfite.

The effect of flow of the test sample on the sensitivity is shown in Fig. 3. From an initial low value with no stirring, the sensitivity rises rapidly with increasing stirring speed and then assumes a steady value. Adequate stirring of the test solution is necessary so that the oxygen concentration (C_s) at the membrane surface would be equal to that of the bulk of the solution.

The linearity of response at 25° $\pm$ 0.5° from zero oxygen to oxygen-saturated solutions is shown in the typical calibration curve of Fig. 4.
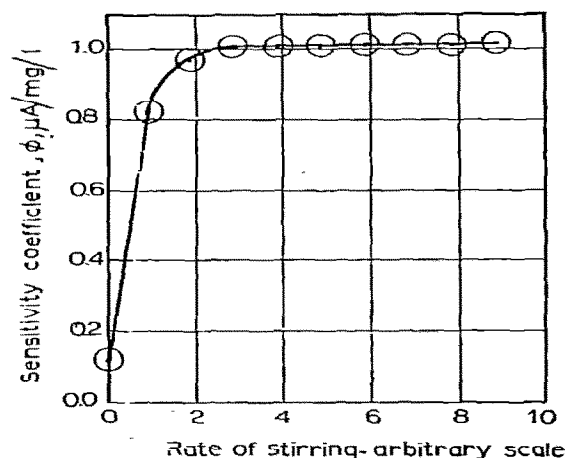

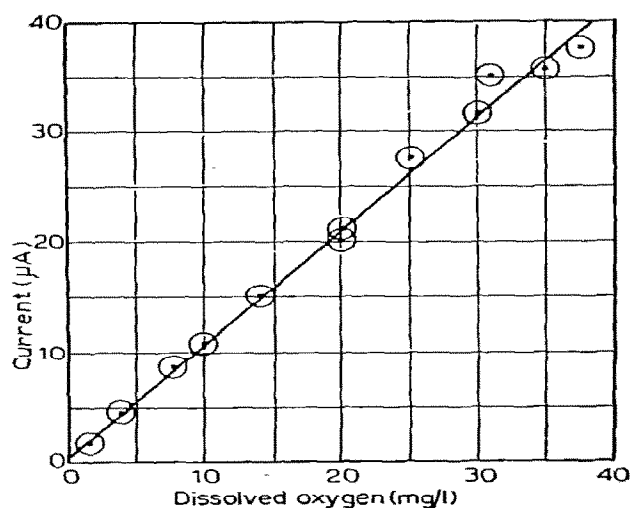Fig. 3. Effect of stirring on sensitivity.

Fig. 4. Dissolved oxygen calibration curve.

Residual current

At zero oxygen concentration in a sample, residual currents are very low, ranging from 0.1 μA to 0.2 μA which corresponds to approximately 0.1–0.2 mg/l. It was originally believed that with each membrane change there would be a new value for the residual current. However, if the membrane is mounted properly and care is taken not to allow air bubbles to be trapped on the electrode surface, the residual current remains at a constant minimum value.

Transient current

During the attainment of a steady state, the current was found to vary inversely with the square root of time. In Fig. 5a the oscilloscope tracing shows the change of current at short time intervals. The logarithmic plot of this current versus time, Fig. 5b, yielded a straight line with a negative slope equal to 0.5 at short times, in

agreement with eqn. 19. The time lag for the attainment of a steady state current was found to be about 3 sec.
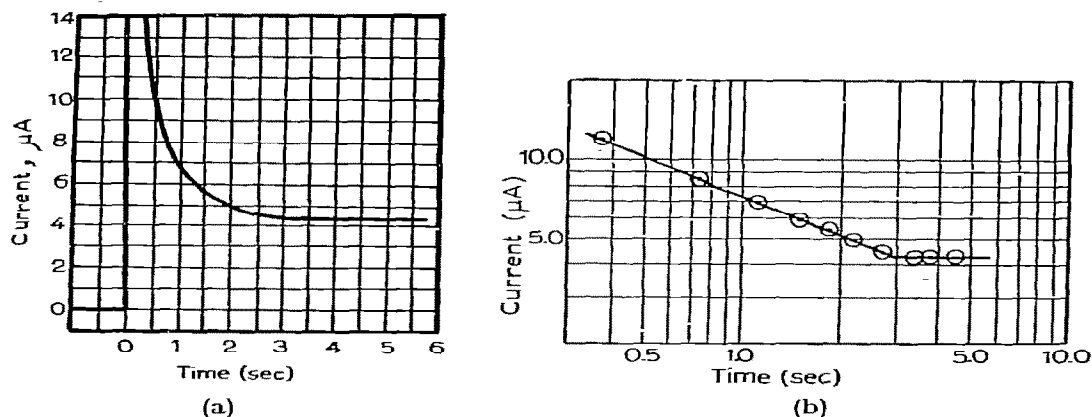

Fig. 5. Transient current: a, current–time curve; b, steady state attainment.

Response time

The response time of the electrode system to changes in oxygen concentrations in aqueous samples is shown in Fig. 6. In Fig. 6a the analyzer was transferred from an air saturated water (8.8 mg/l D.O.) to a deoxygenated water sample. In Fig. 6b the reverse transfer was made. The time lag in response in each direction was 4.9 sec for 90% response, 5.6 sec for 95% response and 7.5 sec for 99% response.

The time lag in response is dependent, of course, on the membrane permeability and thickness and the amount of the electrolytic solution used.
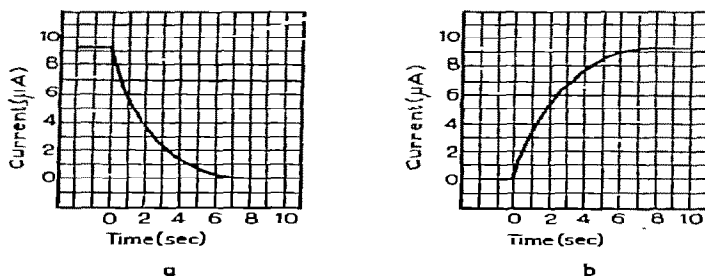

Fig. 6. Response time curve: a, change in concentration from air saturated water to a deoxygenated water sample; b, change in concentration from deoxygenated water to an air saturated water sample.

Temperature coefficient

One of the main characteristics of voltammetric membrane electrodes of this type is their relatively high temperature coefficient. Since the current in these electrode systems is solely dependent on the rate of transport of the electroactive species from the test sample to the electrode surface, the high temperature coefficient is mainly attributable to the permeability characteristics of the plastic membrane.

The lead–silver galvanic cell analyzer was calibrated over a range of oxygen concentrations at 10 temperatures between 5° and 35°. Linear calibrations were

obtained in each case and the sensitivity (slope of calibration curve) is plotted as a function of temperature in Fig. 7a. The sensitivity coefficient, ϕ, $\mu A/mg/l$, was found
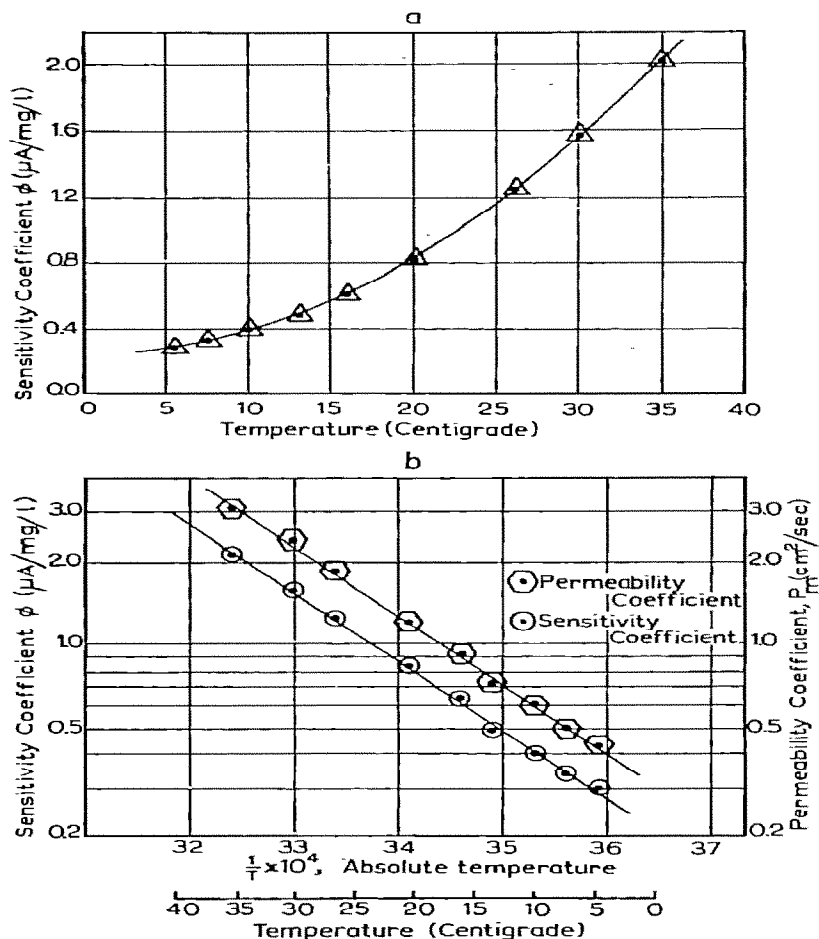

Fig. 7. The effect of temperature on the analyzer sensitivity and the membrane permeability coefficient: a, arithmatic plot of the sensitivity coefficient ϕ versus temperature; b, logarithmic plot of the sensitivity coefficient, ϕ, and the permeability coefficient, P_m, versus temperature.

to vary with temperature according to the classical law of an activated diffusion process:

$$\frac{d\phi}{dT} = \tau \frac{\phi}{T^2} \tag{20}$$

or alternatively

$$\ln \phi = -\frac{\tau}{T} + Q \tag{21}$$

where T is the absolute temperature. A logarithmic plot of the data is presented in Fig. 7b. By means of the plot, giving the change of the sensitivity ϕ with temperature as shown in Fig. 7a, it was then possible to use the analyzer successfully under various temperature conditions.

CARRITT AND KANWISHER[16] used thermistors in their membrane electrode system to compensate for the temperature effects. However, in this study no attempt was made for automatic temperature compensation by means of thermistors because the temperature effect, $d\phi/dT$, is proportional to the permeability coefficient, with the result that any change in the membrane permeability will result in different temperature effects. Plastic membranes even of the same thickness and structural material sometimes show different permeability coefficients from one batch to another depending on the degree of crystallization of the polymer caused by the particular manufacturing process employed. Also on mounting the membrane, a certain amount of stretching is unavoidable and its extent varies with each trial depending on personal technique. Evidently every time the membrane is replaced, there is a great possibility of having a different temperature coefficient and it was found that this factor must always be checked. Nomograph charts such as are shown in Fig. 7b are easy to use for this temperature compensation. One simply determines the sensitivity at a known temperature and plots this point on the Fig. 7b. After drawing a line through this point and parallel to the one already present, the sensitivity at any other temperature can now be read. It is easy to see that a single fixed thermistor *per se* cannot offer adequate temperature compensation.

Membrane permeability

The results of the temperature coefficient in the above section, as well as reported data on gas permeation through plastic membranes[20], indicate that the permeability coefficient increases exponentially with temperature according to:

$$P = P^0 \, e^{-\frac{E_p}{RT}} \tag{25}$$

where E_p is the activation energy of permeation in cal/mole, P^0 the standard permeability coefficient, (corresponding to the frequency factor in the Arrhenius equation), R the universal gas constant in cal/mole deg., and T the absolute temperature.

The permeability coefficient is the product of the distribution coefficient, k, and the diffusion coefficient, D, and both (D and k) vary exponentially with temperature[19,20].

$$D = D^0 e^{-\frac{E_D}{RT}} \tag{30}$$

where E_D is the activation energy of diffusion in cal/mole, and D^0 is the standard diffusion coefficient.

$$k = k^0 e^{-\frac{\Delta H}{RT}} \tag{31}$$

where ΔH is the heat of solution at constant pressure in cal/mole, and k^0 is the standard partition coefficient.

It is important to note that P^0 and D^0 are rate constants while k^0 is an equilibrium constant. The energy of permeation, E_p, is then equal to:

$$E_p = E_D + \Delta H \tag{32}$$

The experimentally determined permeability coefficient of polyethylene membranes

for oxygen at varying temperatures is given in Fig. 7b. In calculating the permeability coefficient, P_m, from the sensitivity, ϕ, the assumption was made that the silver electrode surface area, A, is the effective area for mass transfer and that any edge transport effects are negligible.

The activation energy of permeation is calculated from

$$E_p = 2.303R \log \frac{P_{m_2}}{P_{m_1}} \left(\frac{1}{T_1} - \frac{1}{T_2} \right)$$ (33)

where the subscripts refer to the temperatures, T_1 and T_2. For the polyethylene membranes used in this study the activation energy of permeation was found to be equal to 15,560 cal/mole in good agreement with reported literature values[1].

By means of steady state current measurements using this electrode system or similar designs, it is then possible to study rather easily the oxygen permeability of polymeric membranes. It is believed that this technique is much simpler and more accurate than differential pressure methods.

The salting effect. In the derivation of the theory of diffusion currents, it is assumed that the activity of oxygen is equal to its concentration. However, in cases where the test solution contains high salt concentrations, particularly electrolytes, the activity
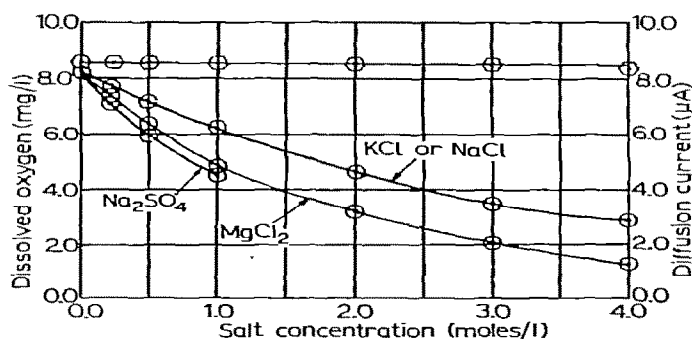

Fig. 8. Diffusion current at various salt concentrations. ⊖, Dissolved oxygen; ◯, diffusion current.

of the oxygen is not equal to the concentration. Although oxygen concentrations in salt solutions in equilibrium with air are lower than those in distilled water samples at the same temperature and oxygen partial pressure, the diffusion current was found to be the same in either case. Fig. 8 shows that the analyzer maintained the same response in air-saturated aqueous systems containing different salt concentrations. Since all solutions were in equilibrium with air under the same temperature and oxygen partial pressure, they had the same oxygen activity. However, the high salt concentration solutions contain lower oxygen concentrations as determined by the WINKLER method[1].

In the case of high salt concentrations, the activity of oxygen is greater than its concentration, which means that its escaping tendency is greater than if the oxygen retains the same properties in the salt solution it possesses in distilled water. The diffusion current of the Galvanic Cell Oxygen Analyzer and similar membrane oxygen analyzers[15,16] measures the activity of oxygen rather than its concentration. Actually,

it is more significant to define oxygen in solution in terms of activity since this is the effective concentration. For instance, activity determines the quantity of oxygen transferable across a respiratory membrane, the oxygen balance in a stream and the rate of corrosion of iron. In the present discussion, oxygen determinations are given in terms of concentration units because of their general acceptance.

When the analyzer is used in water samples containing high salt concentrations such as are encountered in sea water, the concentration of dissolved oxygen could be obtained by multiplying the cell sensitivity by a correction factor. This correction factor is simply the ratio of oxygen solubility in the salt solution to that in distilled water at the same temperature and pressure.

APPLICATIONS

Aeration studies

The galvanic cell oxygen analyzer has been used successfully for determining the role of oxygen transfer in several aeration experiments in laboratory and pilot plant studies.

In bubble aeration processes the electrode system was lowered directly into the aeration column to the desired level. The analyzer was inverted with the surface of the sensing electrode facing upward as in Fig. 9; with this arrangement, the electrode
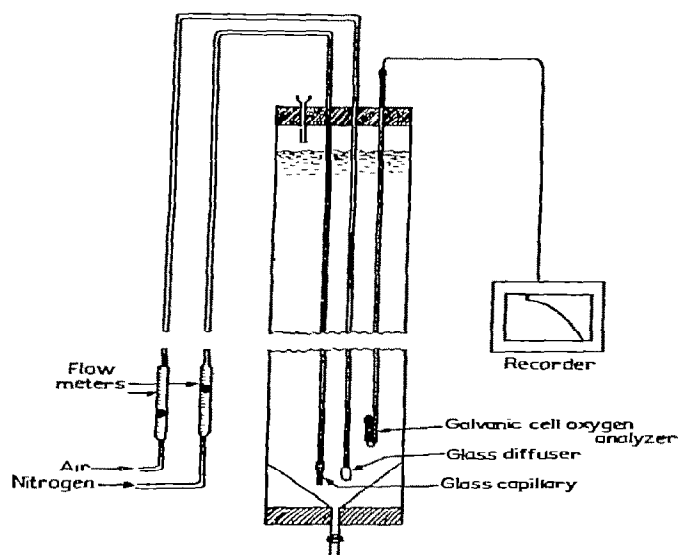

Fig. 9. Apparatus for studying aeration rates.

system could be placed directly in a stream of rising bubbles without interference. Disturbances by natural flow do not affect the analyzer sensitivity since its operating principle is based on achieving adequate stirring in the immediate vicinity of the membrane surface.

When attached to a recorder continuous smooth curves easily read over the normal range of dissolved oxygen concentration were obtained. This procedure permitted convenient measurement of the rate of oxygen transfer in the aeration column without requiring any change of the original volume as a result of sampling.

In aeration experiments where the effect of surface active agents on the rate of oxygen transfer was studied, no effect was found of these added impurities on the analyzer sensitivity.

Oxygen determination in lakes, rivers and other natural water bodies

The simplicity, ruggedness, portability, and ease of handling facilitate the use of the galvanic cell oxygen analyzer under variable field conditions. Being a completely submersible analyzer errors usually caused by sampling difficulties are eliminated since the oxygen is measured *in situ*. This is especially important for studies performed at different depths where changes in the physical and chemical characteristics of depth samples on bringing them to the surface are difficult to circumvent.

Evaluation of a vertical oxygen concentration profile in a fresh water lake

One of the first applications of the galvanic cell oxygen analyzer in the field consisted of obtaining a vertical oxygen profile in a thermally stratified lake. Preliminary tests were first made to evaluate the effect of water pressure on the instrument response. The analyzer was lowered into the lake to different depths and simultaneously samples were pumped up from these levels and analyzed for oxygen using the WINKLER method[1]. The results agreed closely and indicated no apparent effect of
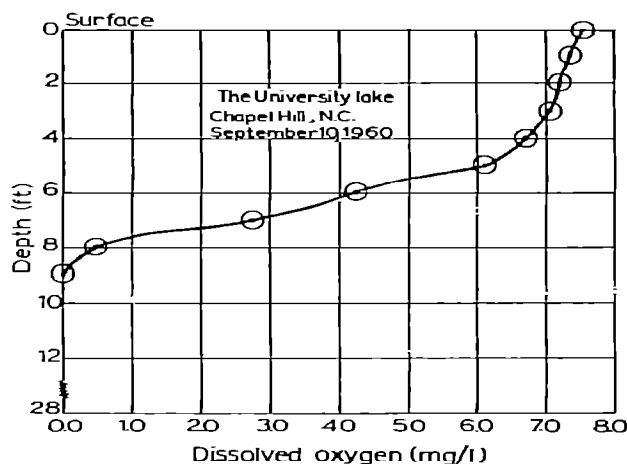

Fig. 10. Dissolved oxygen profile in a thermally stratified lake.

the hydrostatic head on the instrument response throughout the whole depth of the lake (28 ft).

For temperature compensation the analyzer was tied to a telethermometer (Yellow Spring Instrument Co., Inc., Yellow Spring, Ohio) and then lowered in the lake to different depths. Temperature and dissolved oxygen were recorded simultaneously and by means of nomograph charts corrections for temperature were made.

Because the analyzer sensitivity is dependent to a certain extent on the flow characteristics of the test solution, it was then necessary to maintain a certain minimum amount of stirring around the tip of the electrode. In the lake with the analyzer completely submerged in water, a gentle shaking of the attached cable, either man-

ually or by means of a simply automatic device, was sufficient to maintain adequate stirring. In other studies, sufficient stirring was achieved by suspending the analyzer from a moving boat.

Fig. 10 shows a typical dissolved oxygen profile in a thermally stratified lake.

Diurnal changes in dissolved oxygen in a fresh water lake

The oxygen analyzer attached to a telethermometer was lowered in the lake to a predetermined fixed level. The signals were transmitted by means of long cables to the shore where they were recorded continuously on a two channel recorder. In order to maintain a sufficient amount of flow across the membrane, the oxygen analyzer with the telethermometer was placed a few feet in front of a fresh water intake pipe. When the pumping station stopped withdrawing water from the lake during a few hours at night, this was shown clearly on the recorder charts by a decrease in analyzer sensitivity.

Oxygen monitoring in rivers

The galvanic cell oxygen analyzer has been used successfully for monitoring oxygen in streams as a pollution control measure. An example of this case arose when waste from a paper mill was discharged in a river and it was necessary to evaluate the dissolved oxygen relationships downstream. Starting from a point slightly above the waste outlet, the analyzer was lowered in the river from a slowly moving boat and dissolved oxygen and temperature were recorded simultaneously throughout a distance of a few miles downstream. Results showed clearly the effect of the waste on the oxygen balance in the stream and provided valuable information concerning the effect of dilution and reaeration.

Several monitoring stations were then installed to provide a continuous record of dissolved oxygen. This information in turn was used to control the discharge of the plant effluent.

Studies on the rates of oxygen consumption in biological systems

Oxygen uptake rates in biological systems are usually estimated by the manometric method. This method, which is the oldest and best established, consists essentially of allowing the organisms (*e.g.* bacterial suspension) to respire in a closed flask connected to a calibrated manometer. The decrease in pressure inside the flask with time is noted and converted to oxygen uptake rates. Apart from the high cost of the equipment and the fair degree of skill needed for operating the instrument, another serious drawback exists. The measured rate is that of the decrease in the oxygen partial pressure in the gas phase rather than in solution. Hence the observed uptake rate involves the rate of oxygen transfer from the gas to liquid as well as the rate of oxygen consumption in the liquid phase. In cases of high rates of oxygen consumption, the manometrically observed rate is that of transfer of oxygen from gas to liquid rather than the true oxygen consumption of the biological system.

Voltammetric methods on the other hand are capable of detecting the change of oxygen concentration in the liquid phase. While the dropping mercury electrode and platinum electrodes have been applied for this purpose, mercury has been found to exert toxic effects on several biological systems and the adsorption of organic compounds on the electrode surface interfered with the electrode reaction[2-4].

The galvanic cell oxygen analyzer is more suitable for these types of studies and some applications, performed in this laboraotry, are given below.

The rate of oxygen consumption of the nymph of Tetragoneuria cynosura. The metabolic rate during the larval stage of *Tetragoneuria cynosura* was undertaken to identify the various factors influencing the metamorphasis of insects. While most metabolic studies of aquatic larvae employ manometric techniques or microchemical determinations to measure the uptake or evolution of metabolic gases, the galvanic cell oxygen analyzer provides a simpler technique.

A specially designed oxygen analyzer and the respiring nymph were placed in a small cell, and then sealed from contact to the atmosphere. As the nymph respired, the dissolved oxygen concentration in the cell and the corresponding electrode response was recorded continuously. Actually, the decrease of the oxygen concentration with time was due mainly to the respiration of the nymph and to a lesser extent to the electrode reaction. Electrolytic oxygen depletion in the cell could be however calculated from the following relation,

$$C_t = C_0 e^{-Kt} \tag{34}$$

where C_t is the concentration at time t, C_0 is the initial concentration, K is the rate constant in min^{-1} and t is the time in min. The K value was estimated for the electrode system according to,

$$K = 25.8 \frac{P_m A}{vb} \tag{35}$$

where P_m is the membrane permeability coefficient in cm^{2}sec^{-1}, A is the cathode surface area in cm^2, v is the volume of the test solution in cm^3, and b is the membrane thickness in cm.

For a 100 ml cell at 8 mg/l initial oxygen concentration, the decrease in the oxygen in solution by 1 mg/l due to the electrode reaction took about 83 h. Control experiments performed under the same conditions showed also that this effect proceeds at a very slow rate and could be neglected.

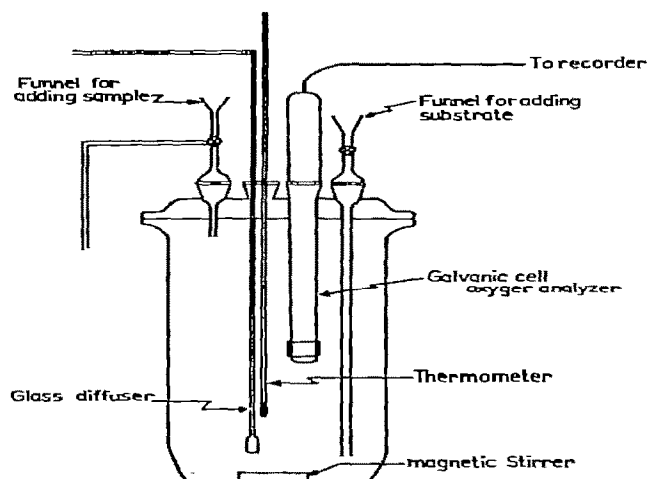Being a completely portable instrument, the galvanic cell oxygen analyzer can

Fig. 11. Respirometer cell assembly.

easily be used for studying respiration rates of different organisms near their own natural environment.

Studies on oxygen utilization of domestic sewage. The oxygen analyzer has been used in this laboratory as the oxygen measuring system in a specially designed respirometer for determining oxygen uptake rates in activated sludge samples. Fig. 11 shows the respirometer cell assembly fitted with facilities for measuring oxygen in solution, for measuring temperature and for adding samples or substrates. The cell assembly was kept at constant temperature in a water bath and the oxygen content was recorded on a potentiometric recorder.

After a sample of the culture was added to the respirometer, it was aerated until stability was reached. The air was then turned off, the stirrer was started, and any change in oxygen concentration in the test solution was recorded. From the recorded data respiration rates were easily calculated.

Oxygen determinations in gaseous systems. Exploratory experiments performed in this laboratory on the application of the galvanic cell oxygen analyzer for oxygen determination in the gaseous phase showed that the current in this case was proportional to the partial pressure of oxygen (Fig. 12). The analyzer response time in gaseous samples was 2.7 sec for 90% response, 5 sec for 95% response, and 25–30 sec for 99% response.
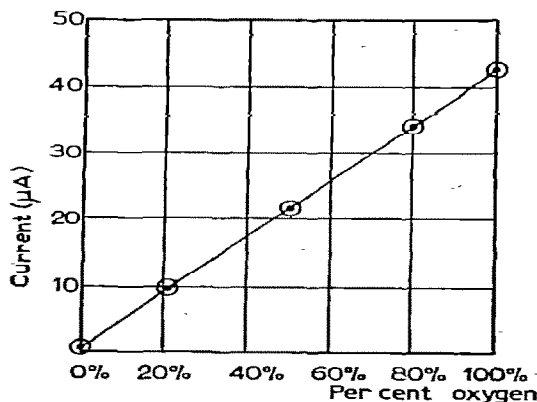

Fig. 12. Oxygen calibration curve in gaseous streams.

The principal difficulty in applying the membrane analyzer to anhydrous gaseous samples was that the electrolyte solution layer eventually dries out since the polyethylene membrane is slightly permeable to water vapor. However, laboratory experiments showed that for 72 h of continuous operation at 27° and at about 82% relative humidity there was no apparent change in the analyzer sensitivity.

APPENDIX

THE MATHEMATICAL TREATMENT OF THE DIFFUSION PROBLEM

According to the model given in Fig. 2, the problem is that of a linear finite diffusion in a two-phase medium. The Laplace transform is used to solve FICK's second law under the prescribed initial and boundary conditions.

By definition the Laplace transform is

$$\mathscr{L}(f) = \bar{f}(p) = \int_0^\infty e^{-pt} f(t)\, dt \tag{A-1}$$

The Laplace transform for the boundary condition d, is

$$\left(\frac{\partial^2}{\partial x^2}\mathscr{L}C_f\right) - \frac{p}{D_f}\mathscr{L}C_f = -\frac{C_{f,0}}{D_f} \tag{A-2}$$

and for the boundary condition e, is

$$\left(\frac{\partial^2}{\partial x^2}\mathscr{L}C_m\right) - \frac{p}{D_m}\mathscr{L}C_m = -\frac{C_{m,0}}{D_m} \tag{A-3}$$

The solution for the differential equation A-2 is then

$$\mathscr{L}C_f = A e^{\sqrt{\frac{p}{D_f}}\cdot x} + B e^{-\sqrt{\frac{p}{D_f}}\cdot x} + \frac{C_{f,0}}{p} \tag{A-4}$$

and the solution for the equation A-3 is

$$\mathscr{L}C_m = G e^{\sqrt{\frac{p}{D_m}}\cdot x} + H e^{-\sqrt{\frac{p}{D_m}}\cdot x} + \frac{C_{m,0}}{p} \tag{A-5}$$

The Laplace transform for the boundary condition c, is

$$D_f\left(\frac{\partial}{\partial x}\mathscr{L}C_f\right)_{x=0} = D_m\left(\frac{\partial}{\partial x}\mathscr{L}C_m\right)_{x=0} \tag{A-6}$$

From A-4 and A-5 we have

$$\sqrt{D_f}(A - B) = \sqrt{D_m}(G - H) \tag{A-7}$$

The Laplace transform for the boundary condition b, is

$$k_0(\mathscr{L}C_f)_{x=0} = (\mathscr{L}C_m)_{x=0} \tag{A-8}$$

and from A-4 and A-5 we have

$$k_0\left(A + B + \frac{C_{f,0}}{p}\right) = \left(G + H + \frac{C_{m,0}}{p}\right) \tag{A-9}$$

Since $C_{f,0}k_0 = C_{m,0}$ at $x = 0$ this simplifies equation A-8 to

$$(A + B) = (G + H)\frac{1}{k_0} \tag{A-10}$$

The Laplace transform for the boundary condition f, is

$$\mathscr{L}(C_m)_{x=b} = \frac{C_s}{p} k_b \tag{A-11}$$

and from equation A-5 we get

$$G e^{\sqrt{\frac{p}{D_m}}\cdot b} + H e^{-\sqrt{\frac{p}{D_m}}\cdot b} + \frac{C_{m,0}}{p} = \frac{C_s}{p} k_b \tag{A-12}$$

Since $C_s k_b = C_{m,0}$, equation A-12 is simplified to

$$G e^{\sqrt{\frac{p}{D_m}} \cdot b} + H e^{-\sqrt{\frac{p}{D_m}} \cdot b} = 0 \tag{A-13}$$

The Laplace transform for the boundary condition a, is

$$\mathscr{L}(C_f)_{x=-a} = 0$$

and from eqn. A-4 we get

$$A e^{\sqrt{\frac{p}{D_f}} \cdot -a} + B e^{-\sqrt{\frac{p}{D_f}} \cdot -a} + \frac{C_{f,0}}{p} = 0 \tag{A-14}$$

On solving the simultaneous eqns. A-7, A-10, A-13 and A-14 for A, B, G, and H we get,

$$A = \tfrac{1}{2} \frac{C_{f,0}}{p} \frac{l e^{\sqrt{\frac{p}{D_m}} \cdot b} - m e^{-\sqrt{\frac{p}{D_m}} \cdot b}}{l \sinh w\sqrt{p} - m \sinh S\sqrt{p}} \tag{A-15}$$

$$B = \tfrac{1}{2} \frac{C_{f,0}}{p} \frac{m e^{-\sqrt{\frac{p}{D_m}} \cdot b} - l e^{\sqrt{\frac{p}{D_m}} \cdot b}}{l \sinh w\sqrt{p} - m \sinh S\sqrt{p}} \tag{A-16}$$

$$G = \frac{C_{f,0}}{p} \frac{e^{-\sqrt{\frac{p}{D_m}} \cdot b}}{l \sinh w\sqrt{p} - m \sinh S\sqrt{p}} \tag{A-17}$$

$$H = \frac{C_{f,0}}{p} \frac{-e^{\sqrt{\frac{p}{D_m}} \cdot b}}{l \sinh w\sqrt{p} - m \sinh S\sqrt{p}} \tag{A-18}$$

Substitution of A and B in eqn. A-4 will give,

$$\mathscr{L}C_f = \frac{C_{f,0}}{p} \left[1 - \frac{m \sinh z\sqrt{p} + l \sinh (-\delta)\sqrt{p}}{l \sinh w\sqrt{p} - m \sinh S\sqrt{p}} \right] \tag{A-19}$$

Also the substitution of H and G in eqn. A-5, will give,

$$\mathscr{L}C_m = \frac{C_{f,0}}{p} \left[k_0 + \frac{2 \sinh \sqrt{\frac{p}{D_m}} (x-b)}{l \sinh w\sqrt{p} - m \sinh S\sqrt{p}} \right] \tag{A-20}$$

The general solution

The next step is to solve for the inverse Laplace transform. Eqn. A-19 may be rearranged as follows,

$$\mathscr{L}C_f = \frac{C_{f,0}}{p} \left[1 - \left\{ \frac{l \sinh (-\delta)\sqrt{p}}{l \sinh w\sqrt{p} - m \sin h S\sqrt{p}} + \frac{m \sinh z\sqrt{p}}{l \sinh w\sqrt{p} - m \sinh S\sqrt{p}} \right\} \right] \tag{A-21}$$

The first term in eqn. A-21 will be treated as follows,

$$\frac{l \sinh (-\delta)\sqrt{p}}{pl \sinh w\sqrt{p} - m \sinh S\sqrt{p}} = \frac{l \sinh (-\delta)\sqrt{p}}{pl \sinh w\sqrt{p}\left(1 - \frac{m}{l}\frac{\sinh S\sqrt{p}}{\sinh w\sqrt{p}}\right)}$$

$$= \frac{l \sinh (-\delta)\sqrt{p}}{p \sinh w\sqrt{p}}\left(1 - \frac{m}{l}\frac{\sinh S\sqrt{p}}{\sinh w\sqrt{p}}\right)^{-1}$$

Since

$$\frac{m}{l}\frac{\sinh S\sqrt{p}}{\sinh w\sqrt{p}} < 1,$$

on expanding

$$\frac{\sinh (-\delta)\sqrt{p}}{p \sinh w\sqrt{p}}\left[1 + \frac{m}{l}\frac{\sinh S\sqrt{p}}{\sinh w\sqrt{p}} + \frac{m^2}{l^2}\frac{\sinh^2 S\sqrt{p}}{\sinh^2 w\sqrt{p}} + \cdots\right] \tag{A-22}$$

The first two terms in the series will be considered only.

The inverse Laplace for $\dfrac{\sinh (-\delta)\sqrt{p}}{p \sinh w\sqrt{p}}$ is[23]

$$\frac{(-\delta)}{w} + \frac{2}{\pi}\sum_{j=0}^{\infty}(-1)^j \frac{\sin\left(\frac{j\pi(-\delta)}{w}\right)}{j}e^{-\left(\frac{j^2\pi^2 t}{w^2}\right)} \tag{A-23}$$

The inverse Laplace for $\dfrac{\sinh S\sqrt{p}}{p \sinh w\sqrt{p}} \cdot \dfrac{\sinh (-\delta)\sqrt{p}}{\sinh w\sqrt{p}}$ is derived as follows:

If $\bar{f}_1(y)$ and $\bar{f}_2(y)$ are the Laplace transforms of $f_1(t)$ and $f_2(t)$ respectively, $\bar{f}_1(y)$, $\bar{f}_2(y)$ are the Laplace transforms of

$$\int_0^t f_1(t-Z)f_2(Z)\mathrm{d}Z = \int_0^t f_1(Z)\cdot f_2(t-Z)\mathrm{d}Z$$

The inverse Laplace for $\dfrac{\sinh S\sqrt{p}}{p \sinh w\sqrt{p}}$, is

$$\frac{S}{w} + \frac{2}{\pi}\sum_{n=0}^{\infty}(-1)^n \frac{\sin\left(\frac{n\pi S}{w}\right)}{n}e^{-\left(\frac{n^2\pi^2 t}{w^2}\right)} \tag{A-24}$$

and the inverse Laplace for $\dfrac{\sinh (-\delta)\sqrt{p}}{\sinh w\sqrt{p}}$ is

$$\frac{1}{w}\frac{\partial\theta_4}{\partial(-\delta)}\left(\frac{(-\delta)}{2w}\bigg/\frac{i\pi t}{w^2}\right)$$

where $\theta_4(\nu/\tau)$ is the theta function[23].

$$\theta_4 = \left(\frac{(-\delta)}{2w} \bigg/ \frac{i\pi t}{w^2}\right) = 1 + 2\sum_{i=0}^{\infty} (-1)^i \left(e^{-\frac{i\pi t \, n^2}{w^2}}\right) \cos\left(2n\pi \frac{(-\delta)}{2w}\right) \frac{1}{w} \cdot \frac{\partial\theta_4}{\partial(-\delta)}$$

$$= \frac{2\pi}{w^2} \sum_{i=0}^{\infty} (-1)^{i+1} e^{-\frac{\pi^2 i^2 t}{t^2}} \sin\left(\frac{i\pi(-\delta)}{w}\right) \quad \text{(A-25)}$$

From eqns. A-24 and A-25, the inverse Laplace for

$$\frac{\sinh S\sqrt{p}}{p \sinh w\sqrt{p}} \cdot \frac{\sinh (-\delta)\sqrt{p}}{\sinh w\sqrt{p}}$$

will be

$$\frac{2\pi}{w^2} \int_0^t \left(\frac{S}{w} + \frac{2}{\pi} \sum_{n=0}^{\infty} (-1)^n \frac{\sin\left(\frac{n\pi S}{w}\right)}{n} e^{-\frac{n^2\pi^2(t-z)}{w^2}}\right) \left(\sum_{i=0}^{\infty} (-1)^{i+1} i \, e^{-\frac{i^2\pi^2 z}{w^2}} \sin\frac{i\pi(-\delta)}{w}\right) dZ \quad \text{(A-26)}$$

The combination of eqns. A-23 and A-26 gives the inverse Laplace for the first term in eqn. A-21, γ_1, which is defined previously in the text (eqn. 9).

The inverse Laplace for the second term in eqn. A-21

$$\frac{m \sinh z\sqrt{p}}{p(l \sinh w\sqrt{p} - m \sinh S\sqrt{p})}$$

is treated in the same manner and the inverse Laplace is given by γ_2 which is also previously defined in the text (eqn. 9).

Accordingly

$$C_f(x,t) = [1 - (\gamma_1 + \gamma_2)] \quad \text{(A-27)}$$

The solution for the inverse Laplace for eqn. A-20 follows also the above treatment,

$$C_m(x,t) = [k_0 - 2\gamma_3] \quad \text{(A-28)}$$

where γ_3 is defined in the text (eqn. 10).

The particular solution

(1) Case of $\dfrac{a}{\sqrt{D_f}} = \dfrac{b}{\sqrt{D_m}}$:

Under this particular condition $S = 0$, $w = 2a/\sqrt{D_f}$ and eqn. A-19 gives

$$\mathscr{L}C_f = \frac{C_{f,0}}{p}\left[1 - \frac{m \sinh z\sqrt{p}}{l \sinh \frac{2a}{\sqrt{D_f}}\sqrt{p}} \cdot \frac{\sinh (-\delta)\sqrt{p}}{\sinh S\sqrt{p}}\right] \quad \text{(A-29)}$$

The inverse Laplace for eqn. A-29 is,

$$C_f(x,t) = C_{f,0}\left[1 - \frac{m}{l}\left(\frac{2}{\pi}\sum_{n-0}^{\infty} \frac{(-1)^n}{n}\sin\frac{n\pi z}{\dfrac{a}{\sqrt{D_f}}}e^{-\frac{n^2\pi^2 t}{n}} + \frac{z}{\dfrac{a}{\sqrt{D_f}}} \right) \right.$$

$$\left. - \frac{(-\delta)}{\dfrac{a}{\sqrt{D_f}}} - \left(\frac{2}{\pi}\sum_{n-0}^{\infty}\frac{(-1)^n}{n}\sin\frac{n\pi(-\delta)}{\dfrac{a}{\sqrt{D_f}}}e^{\frac{n^2\pi^2 t}{\dfrac{a}{\sqrt{D_f}}}} \right) \right] \qquad (A\text{-}30)$$

Similarly eqn. A-20 will give,

$$\mathscr{L}C_m = \frac{C_{f,0}}{p}\left[k_0 + \frac{2}{l}\frac{\sinh\sqrt{\dfrac{p}{D_m}}(x-b)}{\sinh 2\dfrac{a}{\sqrt{D_f}}\sqrt{p}} \right] \qquad (A\text{-}31)$$

and the inverse Laplace, using the theta function, will be

$$C_m(x,t) = C_{f,0}\left[k_0 + \frac{4}{\pi}\frac{1}{l}\sum_{n-0}^{\infty}\frac{(-1)^{n+1}}{n}\sin\left(\frac{n\pi(x-b)}{2a}\sqrt{\frac{D_f}{D_m}} \right)\left(1 - e^{-\frac{n^2\pi^2 D_f t}{4a^2}} \right) \right] \qquad (A\text{-}32)$$

The error function is used to solve for eqn. A-29, which gives

$$C_f(x,t) = C_{f,0}\left[1 - \frac{m}{l}\left\{ \sum_{n-0}^{\infty} 1 - \frac{2}{\sqrt{\pi}}\operatorname{erf} y_1 \right) - \sum_{n-0}^{\infty}\left(1 - \frac{2}{\sqrt{\pi}}\operatorname{erf} y_2 \right) \right\}\right.$$

$$\left. - \left\{ \sum_{n-0}^{\infty}\left(1 - \frac{2}{\sqrt{\pi}}\operatorname{erf} y_3 \right) - \sum_{n-0}^{\infty}\left(1 - \frac{2}{\sqrt{\pi}}\operatorname{erf} y_4 \right) \right\} \right] \qquad (A\text{-}33)$$

where

$$y_1 = \tfrac{1}{2}\left[\frac{2a}{\sqrt{D_f}}(2n+1) - z \right]t^{-\frac{1}{2}}$$

$$y_2 = \tfrac{1}{2}\left[\frac{2a}{\sqrt{D_f}}(2n+1) + z \right]t^{-\frac{1}{2}}$$

$$y_3 = \tfrac{1}{2}\left[\frac{2a}{\sqrt{D_f}}(2n+1) - (-\delta) \right]t^{-\frac{1}{2}}$$

$$y_4 = \tfrac{1}{2}\left[\frac{2a}{\sqrt{D_f}}(2n+1) + (-\delta) \right]t^{-\frac{1}{2}}$$

(2) Case of $\dfrac{a}{\sqrt{D_f}} \gg \dfrac{b}{\sqrt{D_m}}$:

In this case $S = w = a/\sqrt{D_f}$ and eqn. A-19 gives

$$\mathscr{L}C_f = \frac{C_{f,0}}{p}\left[1 - \frac{m\sinh z\sqrt{p} + l\sinh(-\delta)\sqrt{p}}{l\sinh\dfrac{a}{\sqrt{D_f}}\sqrt{p} - m\sinh\dfrac{a}{\sqrt{D_f}}\sqrt{p}} \right] \qquad (A\text{-}34)$$

The inverse Laplace for eqn. A-34, using the theta function, is as follows

$$C_f(x,t) = C_{f,0}\left\{ 1 + \frac{m}{l-m}\frac{2}{\pi}\sum_{n=0}^{\infty}\frac{(-1)^n}{n}\sin\left(\frac{n\pi z\sqrt{D_f}}{a}\right)\left(1 - e^{-\frac{n^2\pi^2 D_f t}{a^2}}\right)\right.$$

$$\left. - \frac{l}{l-m}\left(\frac{\frac{b}{\sqrt{D_m}} - \frac{x}{\sqrt{D_f}}}{\frac{a}{\sqrt{D_f}}} + \frac{2}{\pi}\sum_{n=0}^{\infty}\frac{(-1)^n}{n}\sin n\pi\left(\frac{\frac{b}{\sqrt{D_m}} - \frac{x}{\sqrt{D_f}}}{\frac{a}{\sqrt{D_f}}}\right)e^{-\frac{n^2\pi^2 D_f t}{a^2}}\right)\right\} \quad (A\text{-}35)$$

Similarly eqn. A-20 will give

$$\mathscr{L}C_m = \frac{C_{f,0}}{p}\left[k_0 + \frac{2\sinh\sqrt{\frac{p}{D_m}}(x-b)}{l\sinh\frac{a}{\sqrt{D_f}}\sqrt{p} - m\sinh\frac{a}{\sqrt{D_f}}\sqrt{p}}\right] \quad (A\text{-}36)$$

and the inverse Laplace, using the theta function, is as follows

$$C_m(x,t) = C_{f,0}\left[k_0 - \frac{2}{l-m}\frac{2}{\pi}\sum_{n=0}^{\infty}\frac{(-1)^n}{n}\sin\left(\frac{n\pi(x-b)}{a}\sqrt{\frac{D_f}{D_m}}\right)\left(1 - e^{-\frac{n^2\pi^2 D_f t}{a^2}}\right)\right] \quad (A\text{-}37)$$

On using the error function to solve for eqn. A-34, it follows that

$$C_f(x,t) = C_{f,0}\left\{1 - \frac{m}{l-m}\left[\sum_{n=0}^{\infty}\left(1 - \frac{2}{\sqrt{\pi}}\text{erf }y_1\right) - \sum_{n=0}^{\infty}\left(1 - \frac{2}{\sqrt{\pi}}\text{erf }y_2\right)\right]\right.$$

$$\left. - \frac{l}{l-m}\left[\sum_{n=0}^{\infty}\left(1 - \frac{2}{\sqrt{\pi}}\text{erf }y_3\right) - \sum_{n=0}^{\infty}\left(1 - \frac{2}{\sqrt{\pi}}\text{erf }y_4\right)\right]\right\} \quad (A\text{-}38)$$

(3) Case of $\dfrac{a}{\sqrt{D_f}} \ll \dfrac{b}{\sqrt{D_m}}$:

Under this condition $S = w = b/\sqrt{D_m}$ and eqn. A-19 gives

$$\mathscr{L}C_f = \frac{C_{f,0}}{p}\left[1 - \frac{m\sinh z\sqrt{p} + l\sinh(-\delta)\sqrt{p}}{l\sinh\frac{b}{\sqrt{D_m}}\sqrt{p} - m\sinh\frac{b}{\sqrt{D_m}}\sqrt{p}}\right] \quad (A\text{-}39)$$

As in the previous cases the theta function is used and inverse Laplace will be

$$C_f(x,t) = C_{f,0}\left[1 - \frac{m}{l+m}2\pi\sum_{n=0}^{\infty}\frac{n(-1)^n}{n^2\pi^2}\sin\frac{n\pi z\sqrt{D_m}}{b}e^{-\frac{n^2\pi^2 D_m t}{b^3}}\right.$$

$$\left. - \frac{m}{l+m}\frac{z\sqrt{D_m}}{b} - \frac{l}{l+m}2\pi\sum_{n=0}^{\infty}\frac{n(-1)^n}{n^2\pi^2}\sin\frac{n\pi(-\delta)\sqrt{D_m}}{b}e^{-\frac{n^2\pi^2 D_m t}{b^2}} - \frac{l}{l+m}\left(\frac{(-\delta)\sqrt{D_m}}{b}\right)\right] \quad (A\text{-}40)$$

Eqn. A-20 under the same case will give

$$\mathscr{L}C_m = \frac{C_{f,0}}{p}\left[k_0 + \frac{2\sinh\sqrt{\frac{p}{D_m}}(x-b)}{l\sinh\frac{b}{\sqrt{D_m}}\sqrt{p} + m\sinh\frac{-b}{\sqrt{D_m}}\sqrt{p}}\right] \tag{A-41}$$

and the inverse Laplace

$$C_m(x,t) = C_{f,0}\left[k_0 - \frac{2}{l+m}\frac{2}{\pi}\sum_{n=0}^{\infty}\frac{(-1)^n}{n}\sin\left(\frac{n\pi(x-b)}{b}\sqrt{\frac{D_f}{D_m}}\right)\left(1-e^{-\frac{n^2\pi^2 D_m t}{b^2}}\right)\right] \tag{A-42}$$

The solution of eqn. A-39, using the error function, is

$$C_f(x,t) = C_{f,0}\left\{1 - \frac{m}{l+m}\left[\sum_{n=0}^{\infty}\left(1-\frac{2}{\sqrt{\pi}}\operatorname{erf}y_1\right) - \sum_{n=0}^{\infty}\left(1-\frac{2}{\sqrt{\pi}}\operatorname{erf}y_2\right)\right]\right.$$

$$\left. - \frac{l}{l-m}\left[\sum_{n=0}^{\infty}\left(1-\frac{2}{\sqrt{\pi}}\operatorname{erf}y_3\right) - \sum_{n=0}^{\infty}\left(1-\frac{2}{\sqrt{\pi}}\operatorname{erf}y_4\right)\right]\right\} \tag{A-43}$$

SUMMARY

A galvanic cell consisting of a silver–lead couple separated from the test sample by an oxygen permeable plastic membrane provides the basis of a simple oxygen analyzer. The current generated, while directly proportional to the amount of oxygen in the sample, also depends upon factors such as temperature, membrane thickness, kind and concentration of the supporting electrolyte, and the geometry of the cell. The analyzer has been used successfully with continuous recording devices and as a completely portable instrument with a readout on a microammeter for oxygen monitoring in natural waters and wastes. Oxygen content in non-aqueous systems and gaseous streams may be measured by the device.

REFERENCES

1 *Standard Methods for the Examination of Water, Sewage and Industrial Wastes*, 10th edn., Am. Public Health Assoc., New York, 1955.
2 K. H. MANCY AND D. A. OKUN, *Anal. Chem.*, 32 (1960) 108.
3 E. W. MOORE, J. C. MORRIS AND D. A. OKUN, *Sewage Works J.*, 20 (1948) 1041.
4 W. R. LYNN AND D. A. OKUN, *Sewage and Ind. Wastes*, 27 (1955) 4.
5 W. HUSMANN AND G. STRACKE, *Wasserwirtsch.-Wassertech.*, 48 (1957) 13.
6 F. KIENEWAG, *German Pat. No.* 824,268 (1951); *Chem. Abstr.*, 48 (1954) 10496.
7 P. A. HERSCH, *Anal. Chem.*, 32 (1960) 1030.

8 W. J. Baker, F. J. Combs, T. L. Linn, A. W. Worting and R. F. Wall, *Ind. Eng. Chem.*, 51 (1959) 727.

9 F. A. Keidel, *Ind. Eng. Chem.*, 52 (1960) 490.

10 F. Tödt, *Arch. Metallk.*, 1 (1947) 469.

11 B. Kamienski, *Bull. acad. polon. sci.*, 5 (6A) (1949) 85.

12 L. C. Clark Jr., R. G. Weld and Z. Taylor, *J. Appl. Physiol.*, 6 (1953) 189.

13 R. B. Reeves, D. W. Rennie and J. R. Pappenheimer, *Federation Proc.*, 16 (1957) 693.

14 K. Sugioka and D. A. Davis, *Anesthesiology*, 21 (1960) 135.

15 D. T. Sawyer, R. S. George and R. C. Rhodes, *Anal. Chem.*, 31 (1959) 2.

16 D. E. Carritt and J. W. Kanwisher, *Anal. Chem.*, 31 (1959) 5.

17 J. J. Lingane, *J. Electroanal. Chem.*, 2 (1961) 296.

18 D. T. Sawyer and L. V. Interrante, *J. Electroanal. Chem.*, 2 (1961) 310.

19 A. E. Alexander and P. Johnson, *Colloid Science*, Oxford University Press, London, chap. 28.

20 R. M. Barrer, *Diffusion In and Through Solids*, Cambridge University Press, London, 1941, chaps. 9 and 10.

21 D. W. Brubaker and K. Kammermeyer, *Ind. Eng. Chem.*, 44 (1952) 1465.

22 P. Delahay, *New Instrumental Methods in Electrochemistry*, Interscience, New York, 1954, chap. 9.

23 H. Batman, *Tables of Integral Transforms, Hyperbolic Functions*, vol. I, McGraw-Hill, London, 1954, p. 258, formula No. 31.